Supplementary Information

to the Perspective

Fire Weather Compromises Forestation-reliant Climate Mitigation Pathways

Felix Jäger[1], Jonas Schwaab[1], Yann Quilcaille[1], Michael Windisch[1,2], Jonathan Doelman[3,4], Stefan Frank[5], Mykola Gusti[5], Petr Havlik[5], Florian Humpenöder[2], Andrey Lessa Derci Augustynczik[5], Christoph Müller[2], Kanishka B. Narayan[6], Ryan S. Padrón[1,7], Alexander Popp[2], Detlef van Vuuren[3,4], Michael Wögerer[5], and Sonia I. Seneviratne[1]

[1]Institute for Atmospheric and Climate Science, ETH Zurich, Zurich, Switzerland
[2]Potsdam Institute for Climate Impact Research, Member of the Leibniz Association, Potsdam, Germany
[3]PBL Netherlands Environmental Assessment Agency, The Hague, The Netherlands
[4]Copernicus Institute for Sustainable Development, Utrecht University, Utrecht, The Netherlands
[5]International Institute for Applied Systems Analysis, Laxenburg, Austria
[6]Joint Global Change Research Institute, Pacific Northwest National Laboratory, College Park, USA
[7]Swiss Federal Institute for Forest, Snow and Landscape Research WSL, Birmensdorf, Switzerland

Correspondence: Felix Jäger (felix.jaeger@env.ethz.ch)

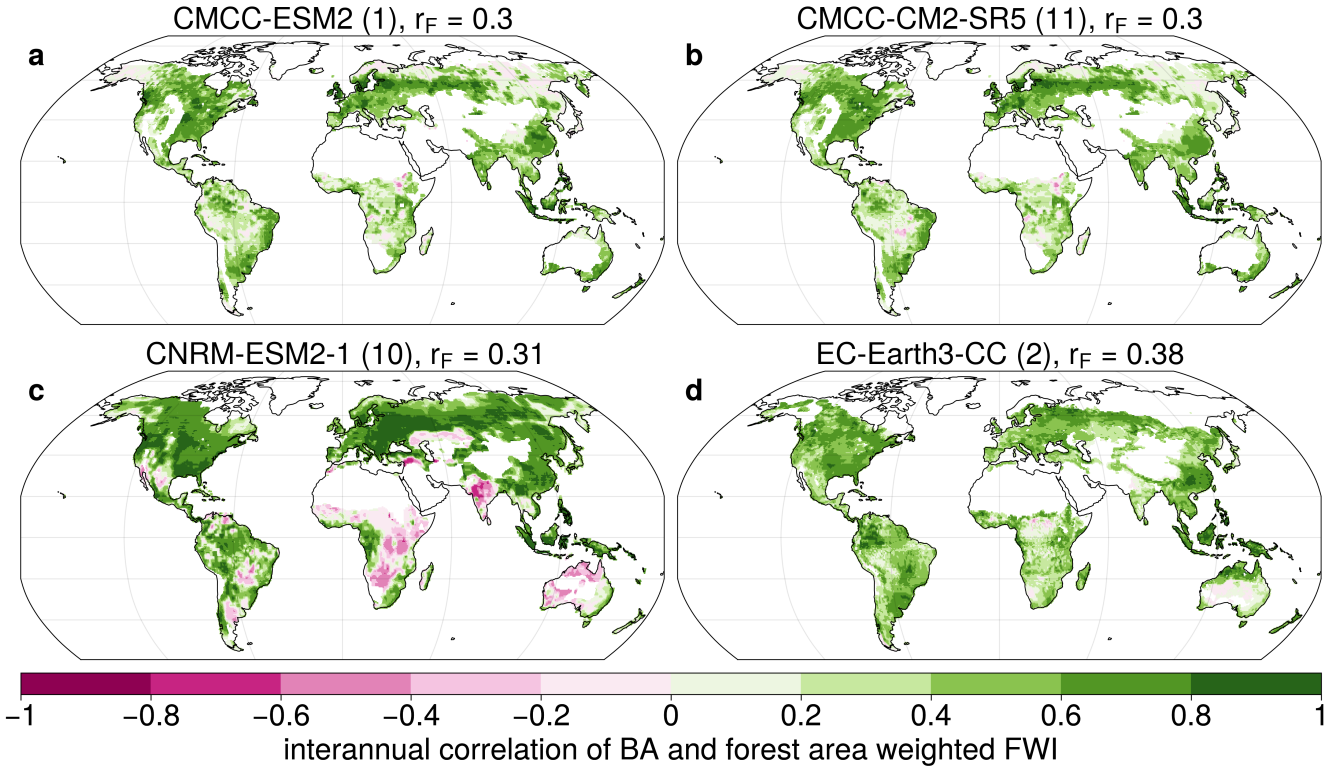

Figure S1. Map of Pearson's correlation of forest area weighted FWI and burned area (BA) in the model experiment 'historical' for four ESMs. In brackets the number of evaluated ensemble members is indicated for each ESM. r_F shown above the map gives the correlation coefficient averaged for grid cells of more than 5 % tree cover according to the land cover map of the respective ESM.

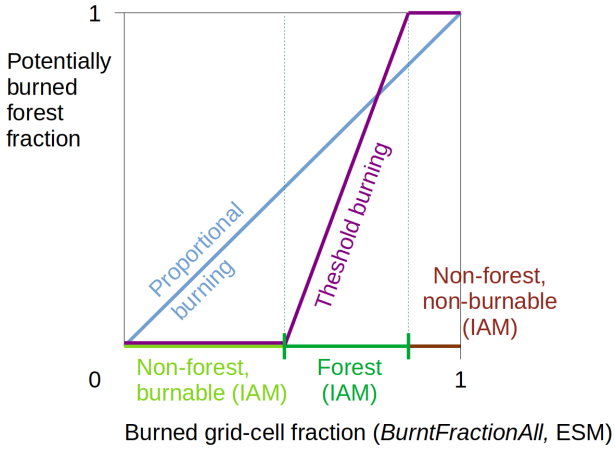

Figure S2. Two possible schemes to determine a fraction of burned forest in IAM land use data sets from the standard variable *BurntFractionAll* from ESMs. For the present analysis, 'threshold burning' was selected, as it follows ecological fire behavior more closely and produces more realistic annual global burned forest areas.

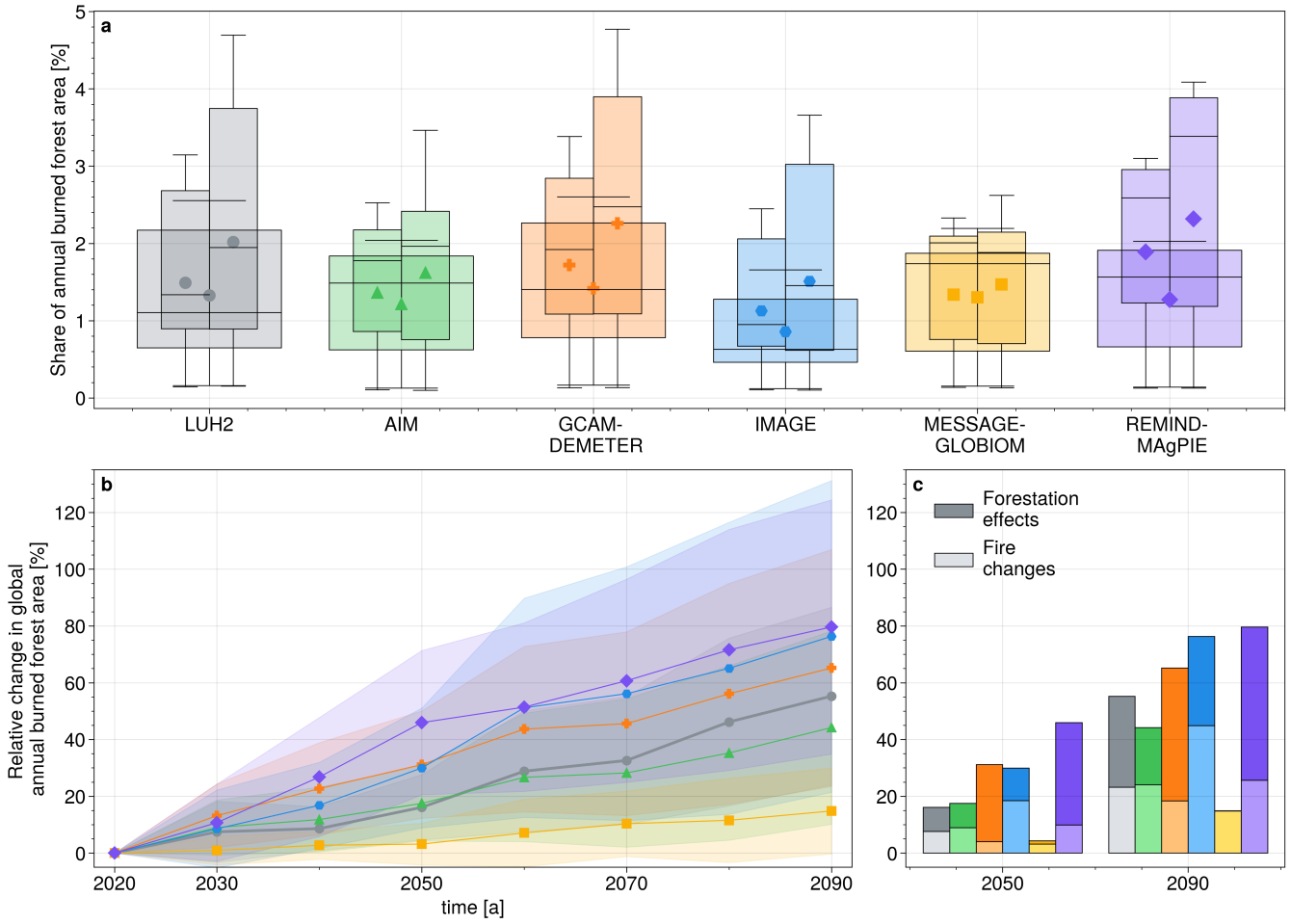

Figure S3. a) Share of annual burned area in all forests in 2020 (wide boxes) and in A/R areas only in 2050 (left) and 2090 (right) under SSP1-2.6 (upper small boxes). The distribution is given by projections of *BurntFractionAll* from 6 Earth System Models. For each IAM, the marker points to the multi-ESM mean, whereas the lines indicate the minimum, 25th, 50th, 75th percentile and the maximum. b) $A_{\text{pot.burned}}$ change relative to 2020 under SSP1-2.6 for different forest projections. The shading indicates one standard deviation from the ESM uncertainty of burned area change. c) Contributions to the relative change in $A_{pot.burned}$ until 2050 and 2090, from forestation (top), and from fire change, (bottom) are shown for the six data sets.

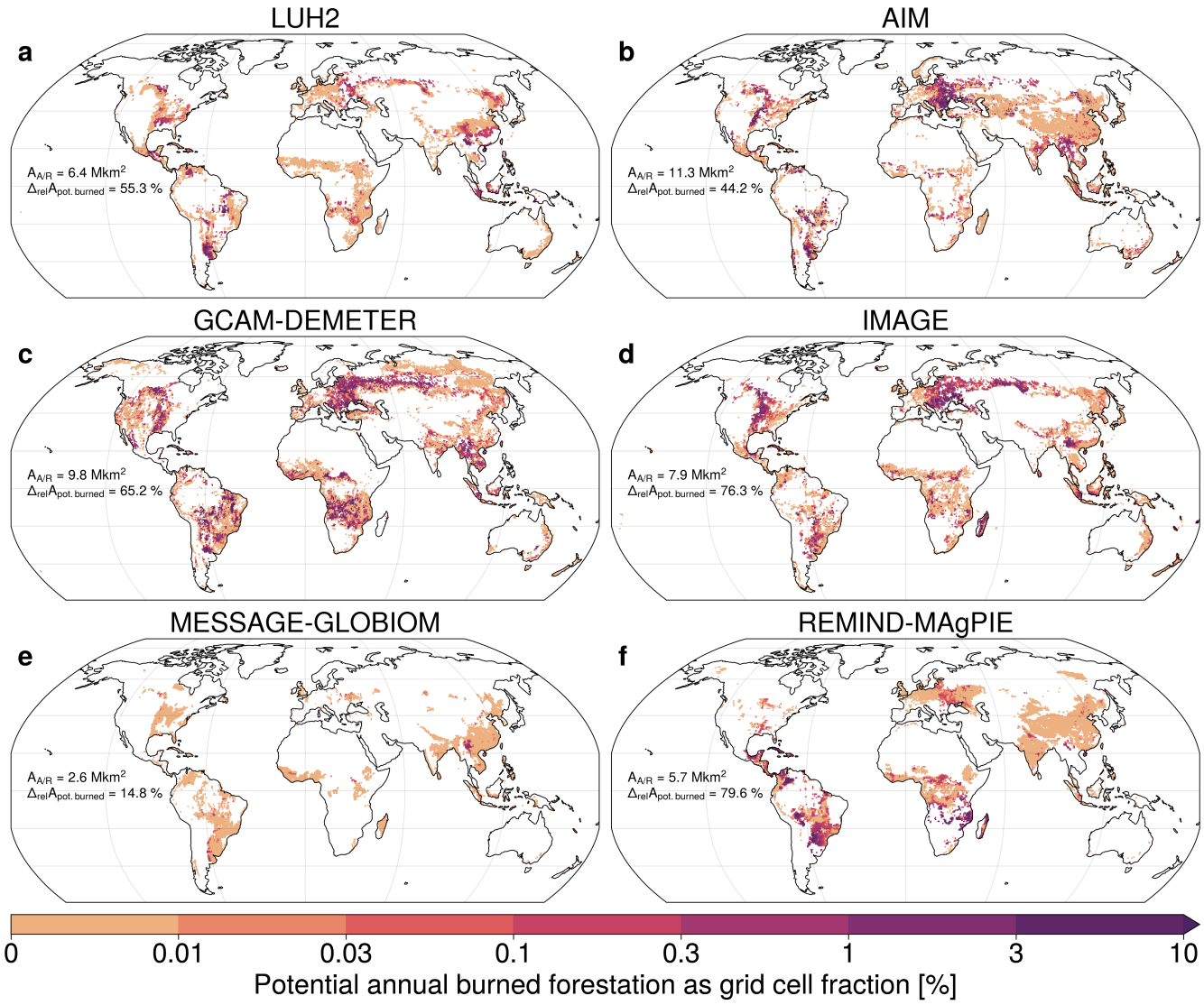

Figure S4. Grid cell fraction of potential annual burned forest area in 2090. $A_{A/R}$ is the overall forestation area since 2020 and $\Delta_{rel}A_{\text{pot.burned}}$ is the relative change in global burned forest area of each model.

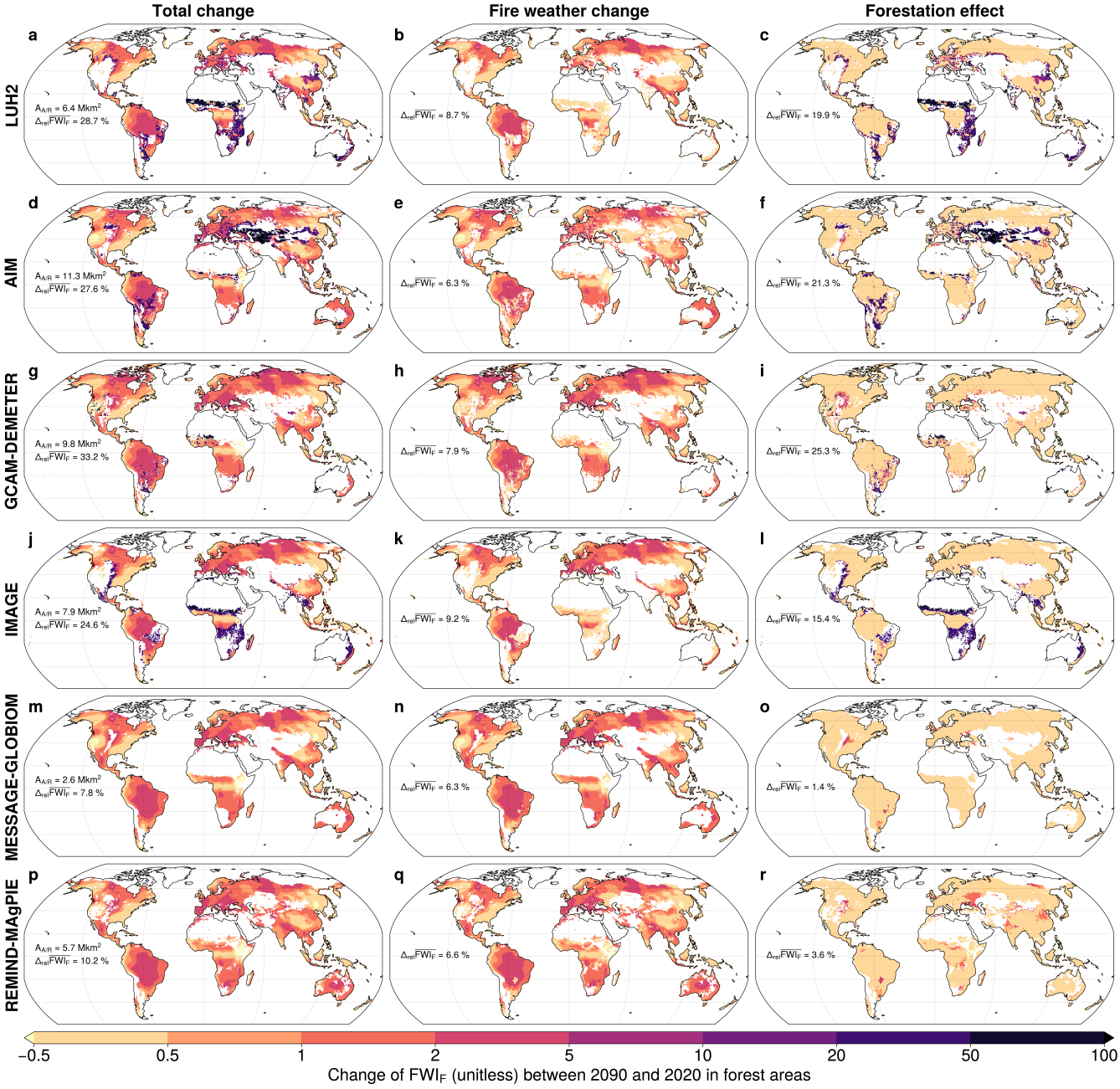

Figure S5. Absolute change in danger (= ·), the product of fire weather index (hazard) and forest grid cell share (exposure) under SSP1-2.6 in 2090 with respect to 2020 in forest areas ($a_F > 5\%$) for LUH2 and five different IAMs. $A_{A/R}$ is the overall forestation area since 2020 and Δ_{rel} is the relative change in global forest weighted mean FWI of each model. The first column gives the overall change, the second column fire weather-induced changes in IAM forest areas in 2020, the third column forestation-induced changes including both the signal of forestation in intense and intensifying fire regimes.

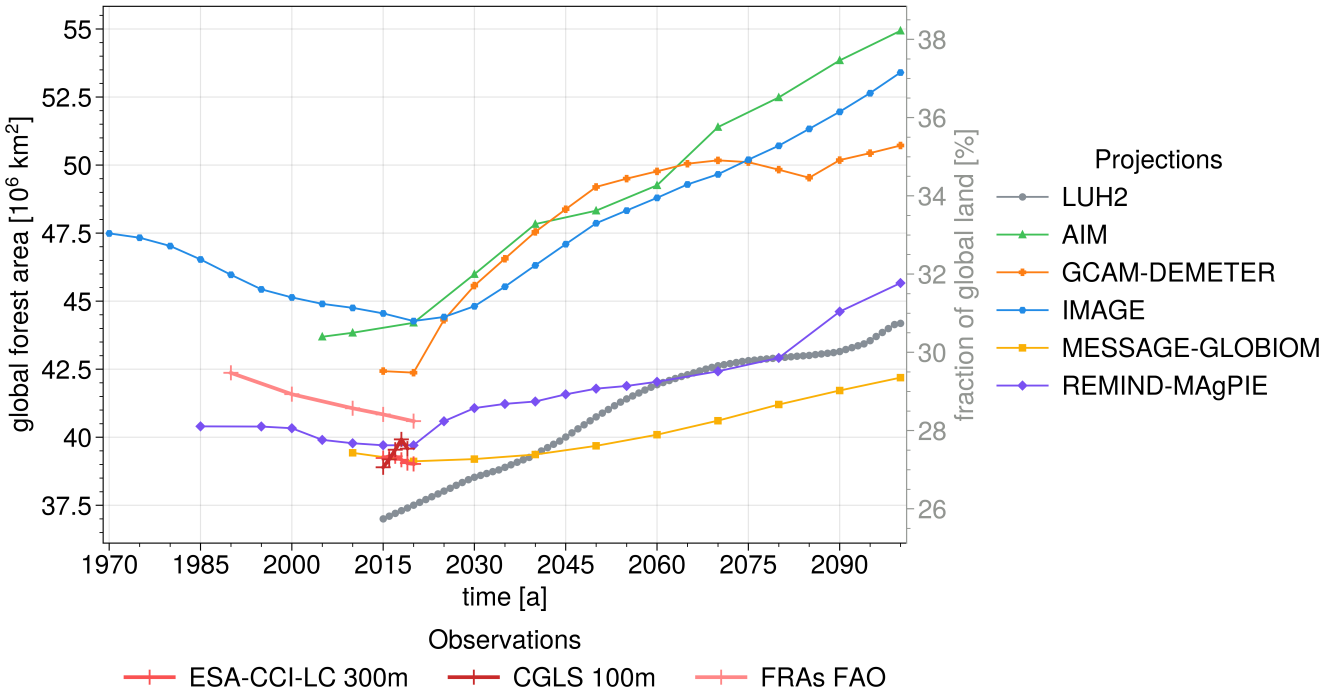

Figure S6. Projected and observed (red) global forest area. Six projections under SSP1-2.6 are shown for LUH2 and five different IAMs. Two observational data sets from satellite imagery (Harper et al., 2023; Buchhorn, 2020) and data from forest resource assessments (FRAs) of the FAO (FAO, 2016; FAO, 2020) are shown for past and present. The diversity of the projections, including start date and time step is shown explicitly for these data sets.

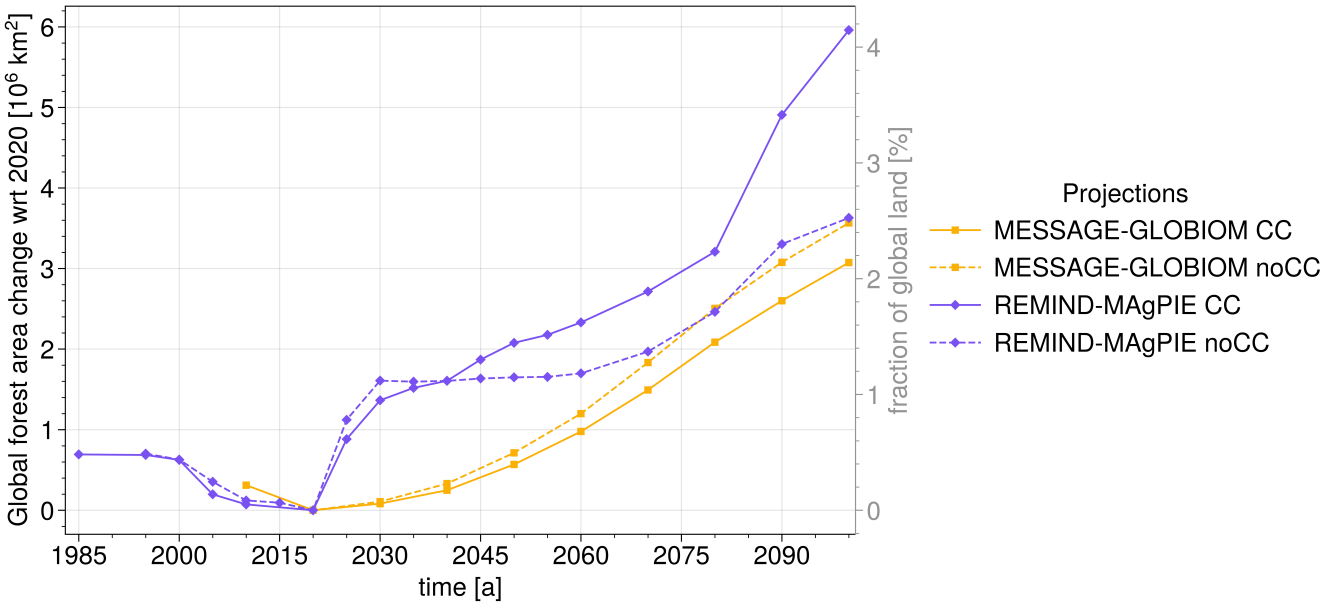

Figure S7. Projected change in global forest area for two simulations, with net climate impacts (CC) and without (noCC). See Methods and section S8 for discussion.

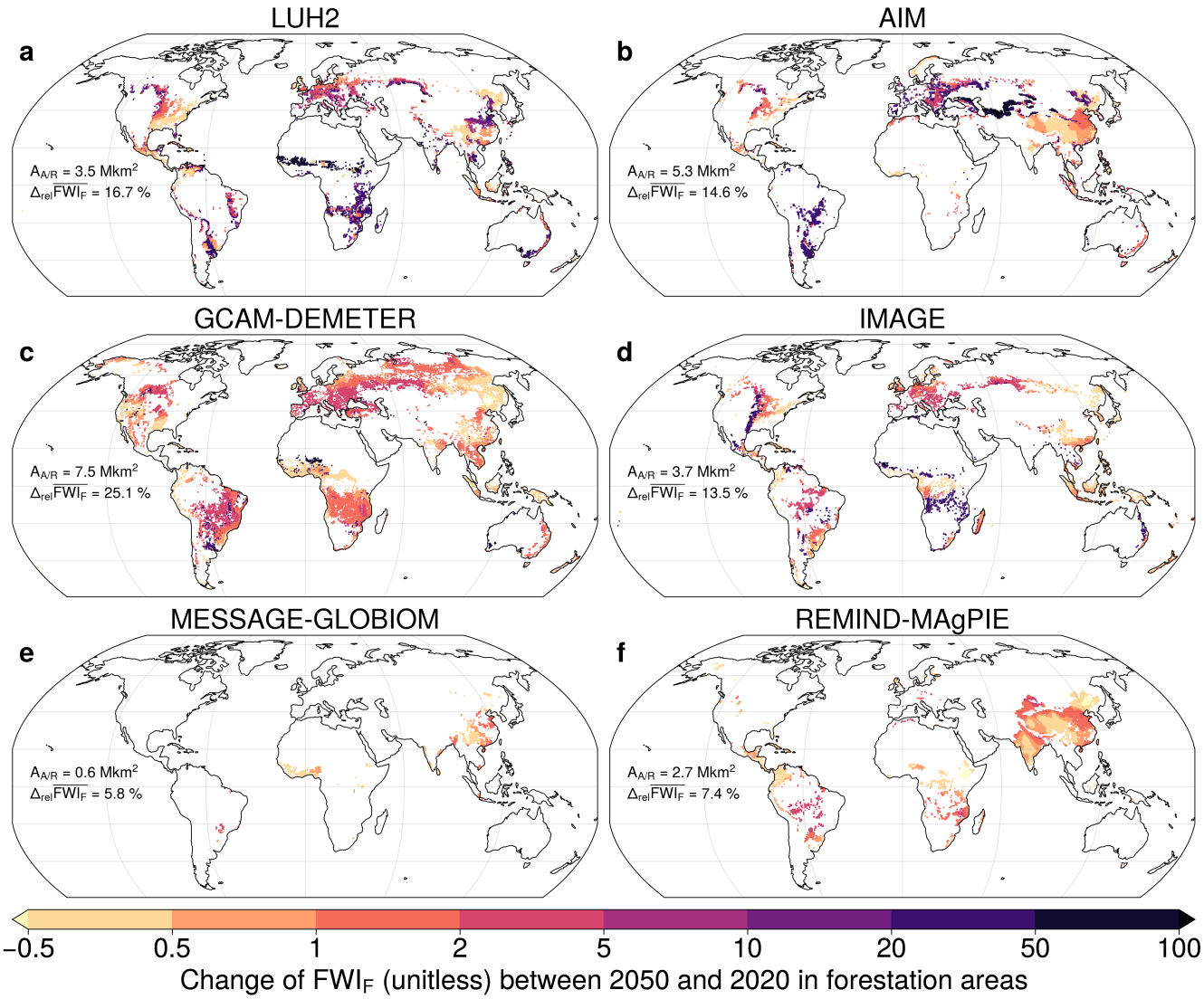

Figure S8. Absolute change in danger (= ·), the product of fire weather index (hazard) and forest grid cell share (exposure) under SSP1-2.6 in 2050 with respect to 2020 in forestation areas ($\Delta > 5\%$) for LUH2 and five different IAMs. $A_{A/R}$ is the overall forestation area since 2020 and Δ_{rel} is the relative change in global forest weighted mean FWI of each model.

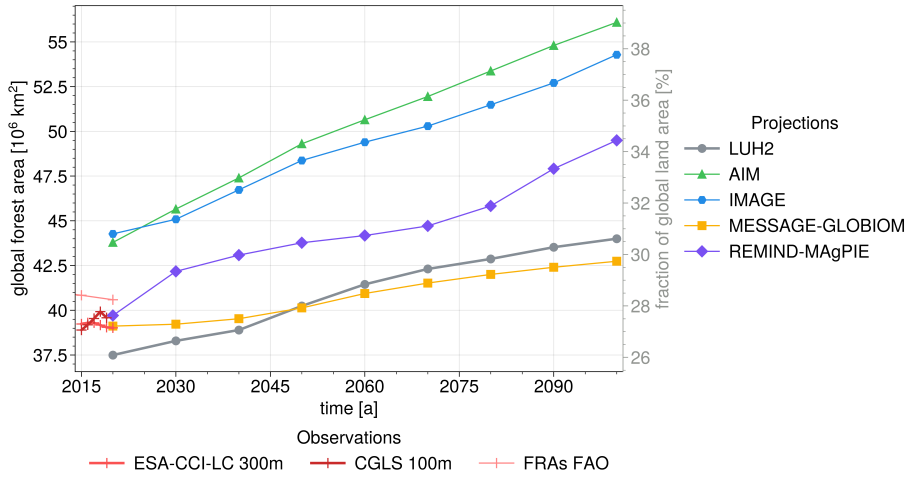

Figure S9. Projected and observed (red) global forest area. Six projections under SSP1-1.9 are shown for LUH2 and five different IAMs. Two observational data sets from satellite imagery (Harper et al., 2023; Buchhorn, 2020) and data from forest resource assessments (FRAs) of the FAO (FAO, 2016; FAO, 2020) are shown for past and present.

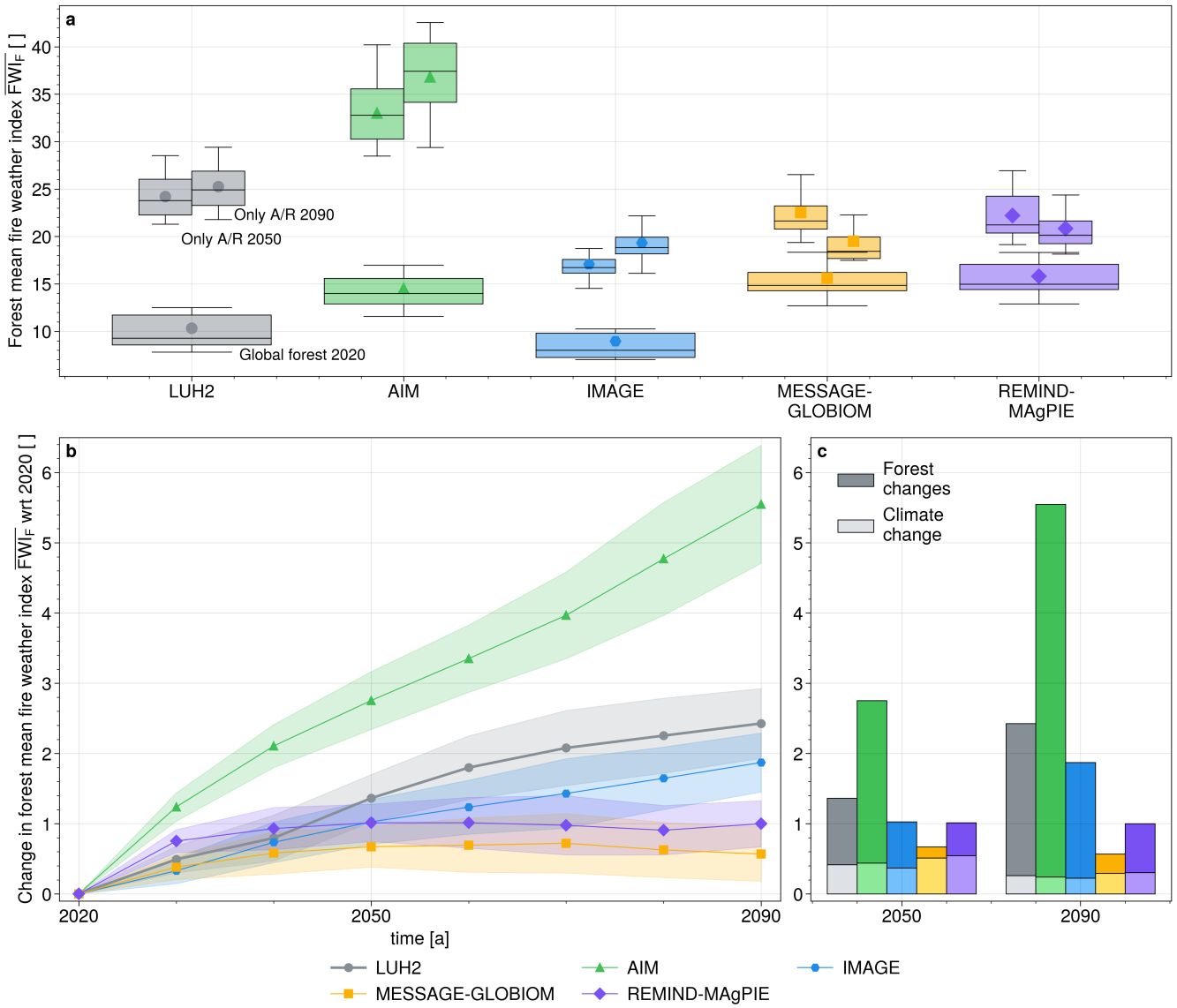

Figure S10. a) in the whole forest in 2020 (wide boxes) and in A/R areas in 2050 and 2090 under SSP1-1.9 (upper small boxes). The vertical distribution is given by ten different fire weather projections. For each IAM, the marker points to the multi-ESM mean. b) change relative to 2020 under SSP1-1.9 for different forest projections. The shading indicates one standard deviation from the ESM uncertainty of FWI change. c) Contributions to the change until 2050 and 2090, forest area changes (top), the fire weather change (driven by climate change, bottom) are shown for the six data sets.

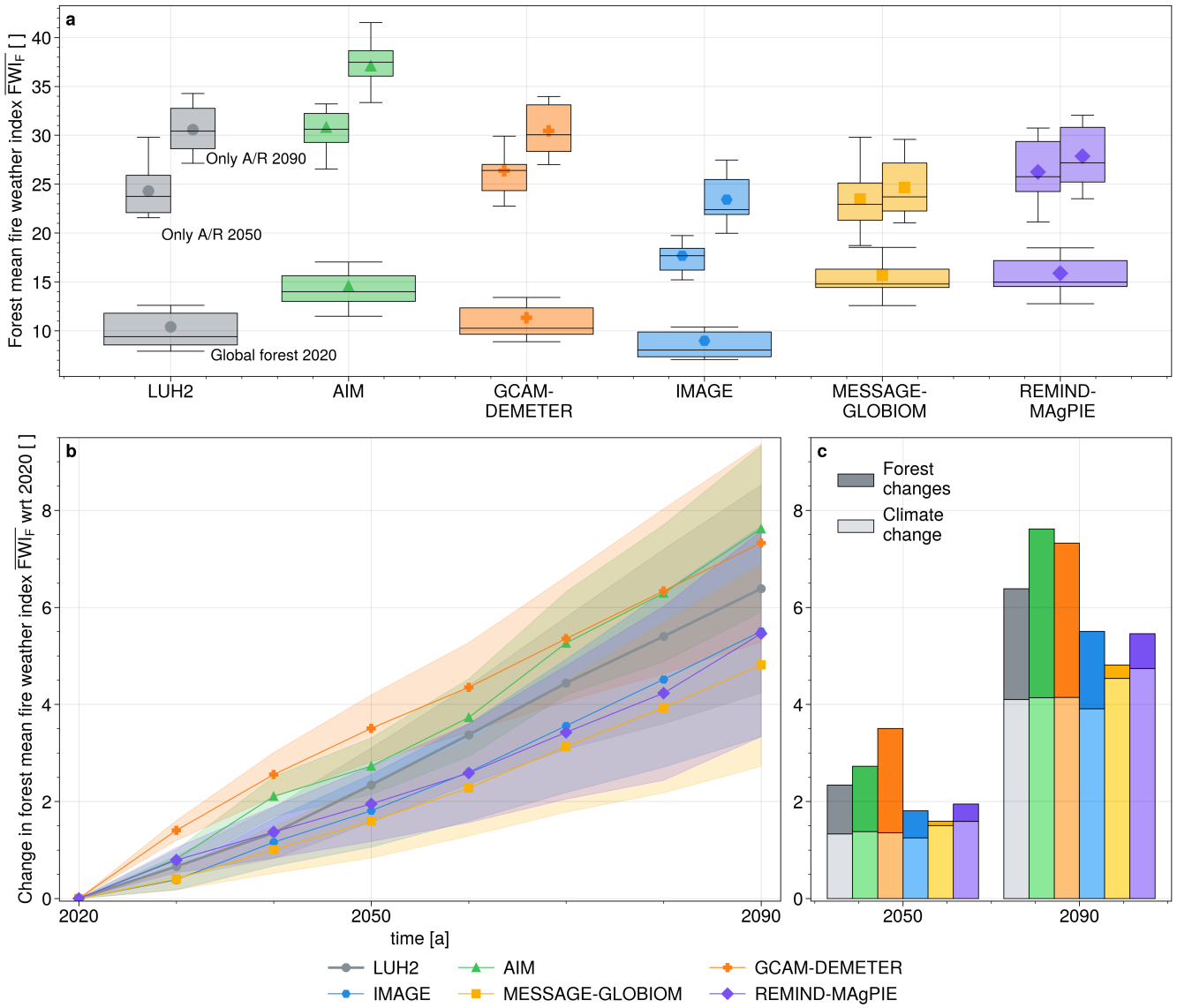

Figure S11. a) in the whole forest in 2020 (wide boxes) and in A/R areas (following SSP1-2.6) in 2050 and 2090 under climate following SSP5-8.5 (upper small boxes). The vertical distribution is given by ten different fire weather projections. For each IAM, the marker points to the multi-ESM mean. b) change relative to 2020 for different forest projections. The shading indicates one standard deviation from the Earth System Model uncertainty of FWI change. c) Contributions to the change until 2050 and 2090, forest area changes (top), the fire weather change (driven by climate change, bottom) are shown for the six data sets.

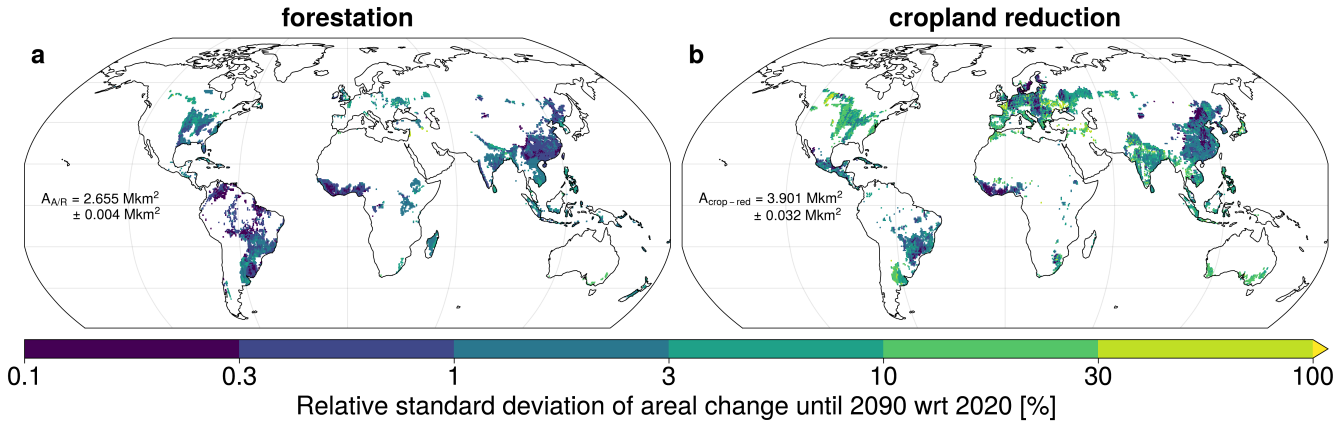

Figure S12. Relative standard deviation in land use change under SSP1-2.6 in 2090 with respect to 2020 as projected by MESSAGE-GLOBIOM under climate impacts from six different ESMs. The values are given for areas, where the mean land use change is affecting more than 5 % of the grid cell. For a discussion, see section S8.

Table S1. Forestation areas $A_{A/R}$ and relative changes in evaluated together as performance measure as ratio of the two values, Ω (see S4 for formula) for A/R allocation in comparably mild fire regimes.

	LUH2	AIM	GCAM-DEMETER	IMAGE	MESSAGE-GLOBIOM	REMIND-MAgPIE
$A_{A/R}$(2050) [Mkm^2]	3.5	5.3	7.5	3.7	0.6	2.7
$A_{A/R}$(2090) [Mkm^2]	6.4	11.3	9.8	7.9	2.6	5.7
Δ_{rel}(2050) [%]	16.7	14.6	25.1	13.5	5.8	7.4
Δ_{rel}(2090) [%]	28.7	27.6	33.2	24.6	7.8	10.2
Ω(2050) [Mkm^2/%]	0.21	0.36	0.30	0.27	0.10	0.37
Ω(2090) [Mkm^2/%]	0.22	0.40	0.29	0.32	0.34	0.56

S1 Fire weather in forests and burned area

is an annual indicator that summarizes atmospheric conditions which are linked to the likelihood of forests to burn. The covariability of fire impacts like burned area and fire carbon emissions with fire weather index, an indicator for fire-promoting atmospheric conditions, has been assessed in numerous studies showing a robust link for long-term continental scale (Bedia et al., 2015; Abatzoglou et al., 2018; Jones et al., 2022). Bedia et al. (2015) report robust correlations of burned area (BA) with FWI in a subset of ESMs within CMIP5. For four ESMs from CMIP6, we study Pearsons interannual correlation of burned area with forest area weighted FWI. Using the definition of tree fractional cover specific to each model the weighted FWI was computed as product with tree fractional area. We find a mean Pearson correlation of 0.3 to 0.38 in partly or fully forested regions (Fig. S1). Only very few vegetated regions show zero or negative correlation and most negative trends in FWI are non robust signals, i.e less than 8/10 ESMs agreeing on signs. We interpret the overall covariance of forest area weighted FWI and burned area as an indication that FWI weighted by forest area is a useful indicator of the risk of burned area in many regions according to the land models used in CESM2 and CESM2-WACCM (CLM5), CMCC-ESM2 and CMCC-ESM2-SR5 (CLM4.5), CNRM-ESM2-1 (ISBA-CTRIP) and EC-Earth3-CC (LPJ-GUESS).

Moreover, the tested the covariability of global burned forest area and global forest area weighted mean FWI for the six data sets. We determined burned forest area assuming grasslands and other natural land as given by the IAM land cover /land use datasets to burn before forest is affected (threshold burning in Fig. S2).

This underlines that is suited to assess fire danger for IAM forest projections, without explicitly estimating burned areas.

For completeness, Fig. S3b,c depict the full uncertainty range of relative change in burned area already shown in Fig. 4d,e in the main text. Additionally we provide maps of burned area for the six assessed data sets in Fig. S4 to provide background on how the global aggregate trends arise.

S2 Decomposition of danger change into contributions from forest cover and fire weather changes

To attribute changes in forest fire danger as measured by

$$\mathrm{FWI_F}(t) = \mathrm{FWI_{SA}}(t) \cdot \mathrm{a_F}(t) \tag{1}$$

to changes in FWI and forest cover separately, we can apply the decomposition of changes into three terms,

$$\Delta\mathrm{FWI_F} = \underbrace{\Delta\mathrm{FWI_{SA}} \cdot \mathrm{a_F}(t_0)}_{\text{i) fire weather changes}} + \underbrace{\mathrm{FWI_{SA}}(t_0) \cdot \Delta\mathrm{a_F}}_{\text{ii) forest cover changes}} + \underbrace{\Delta\mathrm{FWI_{SA}} \cdot \Delta\mathrm{a_F}}_{\text{iii) both change}} , \tag{2}$$

where for any variable X

$$\Delta X = X(t_1) - X(t_0) \, . \tag{3}$$

In the presented analysis we typically combine terms ii) and iii) as here danger increases both from the effect of forest expansion into fire-prone (high $\mathrm{FWI_{SA}}(t_0)$) terrain as well as expansion into regions of intensifying fire weather ($\Delta\mathrm{FWI_{SA}} > 0$) are

attributed to forestation. This leads to the distinction of

$$\Delta \mathrm{FWI_F} = \underbrace{\Delta \mathrm{FWI_{SA}} \cdot \mathrm{a_F}(t_0)}_{\text{i) fire weather change}} + \underbrace{\mathrm{FWI_{SA}}(t_1) \cdot \Delta \mathrm{a_F}}_{\text{ii)' forestation effect}} \tag{4}$$

only as applied in Fig. 4c,e, S5 and S10 .

S3 Further data on forestation areas in SSP1-2.6

Here, we provide more data and background concerning forestation areas under SSP1-2.6, a scenario roughly compatible with two degree global warming. We show global forest area as projected by the six data sets in original temporal coverage (Fig. S6). For details, please refer to the Method section.

Secondly, we provide an illustration of global forest areas over time as projected by two IAMs (MESSAGE-GLOBIOM and REMIND-MAgPIE) under SSP1-2.6 with versus without net climate impacts on land use (Fig. S7).

This figure shows that the mitigation portfolio in IAMs is sensitive to forest carbon potentials altered by climate impacts, being it positively (CO2-fertilization) or negatively (disturbances). Under net climate change impacts, typically dominated by CO2-fertilization in the implementation in IAMs, REMIND-MAgPIE projects a stronger increase in forest area than without. This is mainly because the net positive climate impact on forests is taken into account in this model framework. MESSAGE-GLOBIOM behaves quite the opposite. It only models net climate impacts on agriculture, not on forests, and hence shows an inter-land-type imbalance leading to a weaker expansion of forest under the influence of modeled climate change, because cropland (mainly from CO2-fertilization) becomes a bit more valuable, hence is not so easily transformed into forestation land.

Thirdly, we complement Fig. 5 of the manuscript about 2090 with a corresponding map of forestation distribution and changes in danger in 2050 (Fig. S8).

S4 Global aggregate A/R allocation performance

To illustrate how the different IAMs perform at allocating new forests in a way that the overall danger from fire weather increases only slightly or moderately, we divide forestation area by relative increase of .

$$\Omega = \frac{\mathrm{A}_{A/R}}{\Delta_{rel}} , \qquad [\Omega] = \mathrm{Mkm}^2/\% \tag{5}$$

The higher Ω, the higher the models ability to keep low under forestation. Note that both absolute and relative change of as well as Ω are affected by the model-specific baseline (2020). An IAM with extraordinarily high forest fire danger might show comparably low Ω. Nevertheless, in an assessment combined with (2020), it is a helpful measure to rank IAM forest allocation.

As it can be seen, assessing Ω only, REMIND-MAgPIE, AIM and MESSAGE-GLOBIOM perform best in 2090 (comp. Table S1). However, looking back to Fig. 4 in the article, we see that these three have baseline (2020) values well above LUH2, GCAM-DEMETER and IMAGE. So overall, REMIND-MAgPIE with very high Ω and IMAGE with a good balance between low (2020) and moderate Ω stand out in terms of forest allocation under the pressure of fire weather.

S5 Consistent findings also for low warming in scenario SSP1-1.9

Here, additional figures for the scenario SSP1-1.9 compatible with 1.5 °C maximum global-warming are made available. Fig. S9 shows global forest area over time under this even more ambitious forestation scenario. Fig. S10 indicates the resulting danger changes as measured by . Qualitatively, the results closely resemble SSP1-2.6. With weaker global warming, climate change effects on increasing fire danger become less certain and less important in contrast to even larger A/R areas projected for even more carbon sequestration volume. For SSP1-1.9, no equivalent projection by GCAM-DEMETER is available.

S6 Forestation according to SSP1-2.6 under fire weather according to SSP5-8.5

As sensitivity test we combined afforestation data from SSP1-2.6 with fire weather data from SSP5-8.5, i.e. ambitious afforestation under high global warming. While changes in from afforestation are comparable to the above analysis with climate under the SSP1-2.6 scenario, impacts from intensifying fire weather now dominate the stronger upwards trend in (see Fig. S11).

S7 The role of deforestation in global forest fire danger in SSP1-2.6

Although SSP1-2.6 is a scenario with shared socio-economic and policy assumptions inhibiting deforestation largely (Popp et al., 2017), this kind of land transformation still happens in few areas according to the IAM projections. Until 2090, the collection of here assessed datasets projects deforestation areas around 0.9 (0.01 (MESSAGE-GLOBIOM) to 2 (GCAM-DEMETER)) Mkm^2. Typically, deforestation areas are located in areas showing slightly above-average FWI values (except GCAM-DEMETER with specifically low FWI deforestation regions). Our analysis encompasses not only forestation areas typically inducing a rise in the global average danger (), but also deforestation leading to a decrease in exposure and typically a decrease in . However, overall, the net signal showing clearly positive trends in exposure (forest cover), danger (forest cover combined with FWI) and risk (burned forest area) is dominated by forestation and fire intensification in existing forest areas.

S8 Uncertainty in the multi-model chain of climate change mitigation assessments

Gaining insight on how uncertain future land use is due to climate uncertainties is key for the projection of land-based mitigation strategies. A sensitivity study with IAMs, which are enabled to account for climate impacts on land use, where a spread of climate impacts representing impact uncertainty is given as input, would help to assess the reliability of IAM results. This can be done for example by feeding climate data from an ensemble of ESMs into an IAMs and studying the spread in land use allocation as a response to that. The here assessed version of MESSAGE-GLOBIOM for example has performed such multi-member simulation (See Fig. S12a for variance in forestation projection). This IAM does not represent direct impacts on forestation effectiveness. An experiment with these processes enabled therefor is left for future studies. Still, it 1) exemplifies how climate model uncertainty propagating through IAMs into land use allocation can be assessed with these multi-sectoral models. 2) it shows that the here assessed forestation scenarios - partly for the lack of climate impact representation - do not

show large local or global variance in forest allocation upon climate model uncertainty. Croplands in MESSAGE-GLOBIOM are modeled to be affected by climate impacts (see Table 1 in main text), and in fact global cropland reduction shows largest climate model related variances with values still well below the order of 10 %, at the end of the century (2090) even below 1 % (compare Fig. S12b). This indicates that accounting for climate impact uncertainty typically does not lead to uncertainties at the scale of globally aggregated trends, while it can bring clarity to the regional scale, where impact uncertainty resulting from climate model uncertainty in some context appears to be a significant contributor to land use change uncertainty.

In the framework of climate model intercomparisons like CMIP6, where land use change information from IAMs is used, the model chain would be more consistent when the significant feedbacks, as those from climate impacts on land use, are included and tracked. It is noteworthy that not only biogeochemical processes around carbon uptake but also biogeophysical mechanisms rely on projections of land cover. The latter typically act much more locally, therefor regional-scale uncertainty matters for these processes.

Potential future model experiments could encompass factorial experiments (single impacts on land use and overall economy are switched on and off), simulations with an ensemble of climate models providing impact information on forests, and as a goal at the horizon, a periodically coupled simulation of ESMs and IAMs integrating spatially explicit climate impacts on land use and other sectors. Generally, performing more sensitivity and uncertainty assessments for land use and emission projections could help track-keeping uncertainties along the model chain from IAMs to ESMs for emission pathways and from ESMs back to IAMs for impact assessments.

References

Abatzoglou, J. T., Williams, A. P., Boschetti, L., Zubkova, M., and Kolden, C. A.: Global patterns of interannual climate–fire relationships, Global Change Biology, 24, 5164–5175, https://doi.org/10.1111/gcb.14405, 2018.

Bedia, J., Herrera, S., Gutiérrez, J. M., Benali, A., Brands, S., Mota, B., and Moreno, J. M.: Global patterns in the sensitivity of burned area to fire-weather: Implications for climate change, Agricultural and Forest Meteorology, 214-215, 369–379, https://doi.org/10.1016/j.agrformet.2015.09.002, 2015.

Buchhorn, M., S. B. B. L. D. R. B. L. M. T. N. L. L. T. A.: Copernicus Global Land Service: Land Cover 100m: Version 3 Globe 2015-2019: Product User Manual, Zenodo, https://doi.org/10.5281/zenodo.3938963, 2020.

FAO: Global forest resources assessment 2015 : how are the world's forests changing?, ISBN 9789251092835, https://doi.org/10.1016/j.foreco.2015.02.006, 2016.

FAO: Global Forest Resources Assessment 2020, FAO, https://doi.org/10.4060/ca9825en, 2020.

Harper, K. L., Lamarche, C., Hartley, A., Peylin, P., Ottlé, C., Bastrikov, V., San Martín, R., Bohnenstengel, S. I., Kirches, G., Boettcher, M., Shevchuk, R., Brockmann, C., and Defourny, P.: A 29-year time series of annual 300 m resolution plant-functional-type maps for climate models, Earth System Science Data, 15, 1465–1499, https://doi.org/10.5194/essd-15-1465-2023, 2023.

Jones, M. W., Abatzoglou, J. T., Veraverbeke, S., Andela, N., Lasslop, G., Forkel, M., Smith, A. J. P., Burton, C., Betts, R. A., van der Werf, G. R., Sitch, S., Canadell, J. G., Santín, C., Kolden, C., Doerr, S. H., and Le Quéré, C.: Global and Regional Trends and Drivers of Fire Under Climate Change, Reviews of Geophysics, 60, e2020RG000 726, https://doi.org/10.1029/2020RG000726, 2022.

Popp, A., Calvin, K., Fujimori, S., Havlik, P., Humpenöder, F., Stehfest, E., Bodirsky, B. L., Dietrich, J. P., Doelmann, J. C., Gusti, M., Hasegawa, T., Kyle, P., Obersteiner, M., Tabeau, A., Takahashi, K., Valin, H., Waldhoff, S., Weindl, I., Wise, M., Kriegler, E., Lotze-Campen, H., Fricko, O., Riahi, K., and Vuuren, D. P.: Land-use futures in the shared socio-economic pathways, Global Environmental Change, 42, 331–345, https://doi.org/10.1016/j.gloenvcha.2016.10.002, 2017.